Supporting Information

Adsorption sites engineering: Cu-Ni(OH)$_2$ sheet for Efficient Hydrogen Evolution

Wenda Zhong[a], Chenfan Yang[a], Jing Wu[a], Wenli Xu[b], Rong Zhao[b], Hui Xiang[b,], Ke Shen[a,]*, and Xuanke Li[a,b,]**

[*] Prof. X. K. Li, [*] Prof. K. Shen, [*] Prof. H. Xiang, W. D. Zhong, C. F. Yang, J. Wu, W. L. Xu, R. Zhao
Hunan Province Key Laboratory for Advanced Carbon Materials and Applied Technology, College of Materials Science and Engineering, Hunan University, Changsha, Hunan 410082, China
E-mail: xkli8524@sina.com (Xuanke Li)
E-mail: shenk@hnu.edu.cn (Ke Shen)
Hubei Province Key Laboratory of Coal Conversion and New Carbon Materials, School of Chemistry and Chemical Engineering, Wuhan University of Science and Technology, Wuhan, Hubei 430081, China
E-mail: hxiang0717@163.com (Hui Xiang)

Experimental Section

Synthesis of Ni(OH)$_2$/NF: Nickel foam (NF) with an area of 3×3 cm^2 was ultrasonically washed with ethanol, hydrochloric acid (1 M), and ultrapure water for 10 minutes, respectively. Treated NF was then transferred into Teflon-lined stainless reactors (100 mL) containing 80 mL diluted hydrogen peroxide (4.5 wt%). After the hydrothermal oxidation reaction at 160 °C for 6 h., uniform plate-like Ni(OH)$_2$ arrays are generated on NF.

Fabrication of Cu-Ni(OH)$_2$/NF: NF with an area of 3×3 cm^2 was ultrasonically washed with ethanol, hydrochloric acid (1 M), and ultrapure water for 10 minutes, respectively. Treated NF was then transferred into Teflon-lined stainless reactors (100 mL) containing 80 mL diluted hydrogen peroxide (4.5 wt%) and copper nitrate (0.01 mmol). After the hydrothermal reaction at 160 °C for 6 h., Cu-Ni(OH)$_2$ plates are generated on

NF. The Cu/Ni ratio of the Cu-$Ni(OH)_2$ plates is ascertained as about 1% by Inductively Coupled Plasma Optical Emission Spectrometer (ICP-OES). In our verification test, serial Cu-$Ni(OH)_2$/NF samples are fabricated by controlled copper nitrate. ICP-OES measures the Cu/Ni ratios of the Cu-$Ni(OH)_2$ plates. Then, the integrated serial electrodes are denoted as Cu-$Ni(OH)_2$/NF (0.5%), Cu-$Ni(OH)_2$/NF (3%), and Cu-$Ni(OH)_2$/NF (5%), respectively.

Material characterizations: The phase compositions of the samples are investigated by using X-ray diffraction (XRD, TD-3300) with Cu Ka radiation at a scanning step of 5 $°\cdot min^{-1}$. Raman (DXR2) is also conducted to explore the structure of samples. UV-Vis Adsorption spectra obtained from Lambda750 PE. The specific surface area was measured by nitrogen adsorption isotherms (ASAP 2020, Micromeritics) based on Brunauer-Emmett-Teller (BET) model. Furthermore, scanning electron microscopy (SEM, Sigma HD) and transmission electron microscopy (TEM, Tecnai G2 F20 S) are used to study the catalysts' micro-morphology and atomic structure. Energy-dispersive X-ray spectroscopy (EDX) system attached to TEM and X-ray photoelectron spectroscopy (XPS, Thermo ESCALAB 250XI) systems is used to obtain the elemental composition and bonding characteristics of the catalysts. Ultraviolet photoelectron spectra (UPS) measurements are also carried out on ESCALAB 250. ICP-OES is measured by the Agilent 5110 ICP-OES.

Electrochemical measurements: We use Gamry Interface 1000E electrochemical workstation to perform all the electrochemical tests using a standard three-electrode cell, where the self-supporting catalysts are used as the working electrodes, and

Hg/HgO and carbon rod are used as reference and counter electrodes, respectively. The commercial Pt/C catalyst (20 wt%) adheres to nickel foam with the same loading (0.9 mg cm^2) as the comparison sample. Linear sweep voltammetry (LSV) measurements are conducted in a 1M KOH electrolyte. The stability of the catalyst is evaluated by using chronoamperometry. The Tafel slopes are obtained from the LSV plots with a scan rate of 5 mV s^{-1}. All polarization curves are subjected to *iR* compensation. All the potentials are calibrated with respect to a reversible hydrogen electrode (RHE) by adding a value of 0.926 V. Electrochemical impedance spectroscopy (EIS) has conducted at 100 mV with a 5 mV AC potential from 100 000 to 0.01 Hz.

Electrochemical Measurements:

The electrochemical surface area (ECSA) is estimated by cyclic voltammogram (CV) in a small potential range at the different scan rates of 20, 40, 60, 80, and 100 mV s^{-1}. The current density differences are plotted against scan rates, and the linear slope is twice the double-layer capacitance (C_{dl}). Moreover, the roughness factor (R_f) is calculated by the following equation: $R_f = C_{dl}/C_o$, in which C_o is the capacitance of ideal planar metal oxides with smooth surfaces (0.040 mF cm^{-2}). ECSA can be calculated from C_{dl} using the specific capacitance value for a flat standard with 1 cm^2 of the whole surface area. Herein, the NF is used as the standard. ECSA is calculated as follows:

$$A_{ECSA}^{catalyst} = \frac{C_{dl}^{catalyst}(\text{mF cm}^{-2})}{C_{dl}^{NF}\left(\text{mF cm}^{-2}\right) \text{ per cm}_{ECSA}^{2}}$$

Computational configurations

In this work, we used first-principles calculations based on the density function theory (DFT) as implemented in the Vienna Abinitio Simulation Package (VASP) with Projector Augmented Wave (PAW) method.[1] And the exchange-correlation energy is described by the functional of Perderw-Burke-Ernzerhof (PBE) from including van der Waals corrections (DFT-D3 method). The kinetic energy cutoff of electron wave functions is 500 eV. The geometry optimizations are performed by using the conjugated gradient method, and the convergence threshold is set to be 10^{-4} eV in energy and 0.01eV $Å^{-1}$ in force. A vacuum layer of 15 Å is applied for all calculated models.[2] CI-NEB (climbing image nudged elastic band) was used for the transition state searching. Brillouin zone was sampled by a 3×1×1 k-points grid for the structure optimizations and 3*3*1 were employed for the density of states (DOS) calculations, respectively. The Adsorption energy of H_2O was calculated as follows, $\Delta E H_2O = E\text{surf-}H_2O - E\text{surf} - EH_2O$, in which Esurf-H_2O is the total energies of the surface covered with H_2O molecule and Esurf without H_2O molecule, and EH_2O is the energy of free H_2O molecule. The free energies are determined by the following formula $\Delta G = \Delta E + \Delta ZPE - T\Delta S$, where ΔE, ΔZPE, and ΔS represent the binding energy, zero-point energy change, and entropy change of the adsorption of adsorbates, respectively. The related zero-point energies and entropies of H_2, H_2O, H^*, and OH^* are from previous literature.[3,4]

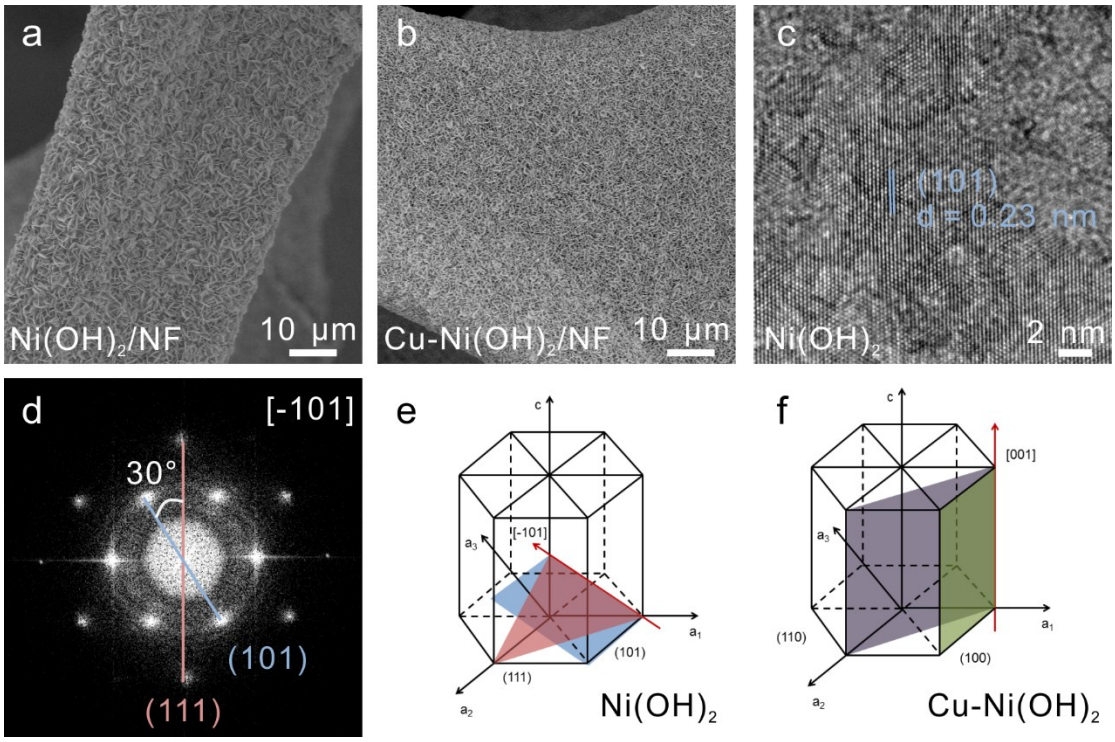

Fig. S1. SEM images of (a) $Ni(OH)_2$/NF and (b) Cu-$Ni(OH)_2$/NF. (c) HR-TEM image and (d) corresponding SAED image of individual $Ni(OH)_2$ plate. Corresponding zone axis of (e) $Ni(OH)_2$ and (f) Cu-$Ni(OH)_2$.

Table S1. Specific surface areas

Sample	BET Surface
NF	0.26 $m^2\ g^{-1}$
$Ni(OH)_2$/NF	0.59 $m^2\ g^{-1}$
Cu-$Ni(OH)_2$/NF	0.89 $m^2\ g^{-1}$

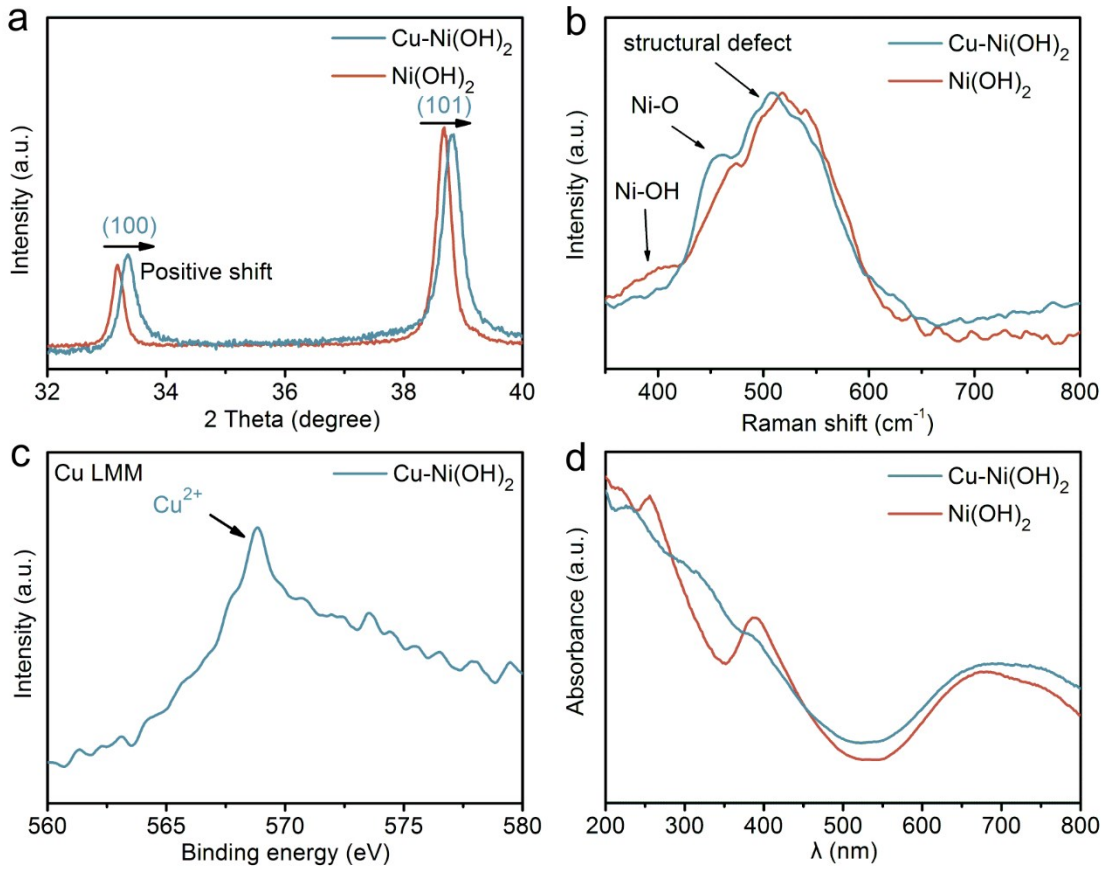

Fig. S2. (a) Enlarged XRD patterns of Cu-Ni(OH)$_2$ and Ni(OH)$_2$. (b) Raman patterns of Cu-Ni(OH)$_2$ and Ni(OH)$_2$. (c) The Cu LMM auger spectrum of Cu-Ni(OH)$_2$. (d) UV-Vis Adsorption spectra of Cu-Ni(OH)$_2$ and Ni(OH)$_2$.

Table S2. Binding energy values from XPS spectra and corresponding Content.

Sample	B.E.(eV)	Content (%)
$Ni(OH)_2$	(Ni^{2+}) 855.45	(Ni 2p) 37.14
	(Ni^{3+}) 856.92	(Ni 2p) 15.05
	(Sat. 1) 861.39	(Ni 2p) 43.20
	(Sat. 2) 866.09	(Ni 2p) 4.61
	(Ni-OH) 531.02	(O 1s) 94.66
	(adsorbent) 532.47	(O 1s) 5.34
Cu-$Ni(OH)_2$	(Ni^{2+}) 855.33	(Ni 2p) 38.00
	(Ni^{3+}) 856.90	(Ni 2p) 13.82
	(Sat. 1) 861.27	(Ni 2p) 43.14
	(Sat. 2) 865.96	(Ni 2p) 5.04
	(Ni-OH) 530.84	(O 1s) 88.74
	(adsorbent) 532.03	(O 1s) 11.26
	(Cu^{+}) 932.73	(Cu 2p) 9.83
	(Cu^{2+}) 934.32	(Cu 2p) 56.27
	(Sat. 1) 941.12	(Cu 2p) 23.45
	(Sat. 2) 943.69	(Cu 2p) 10.45

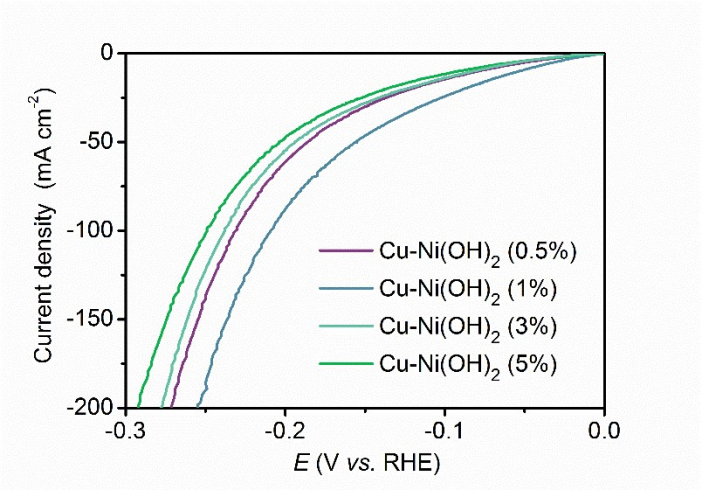

Fig. S3. Polarization curves of serial Cu-Ni(OH)$_2$/NF samples.

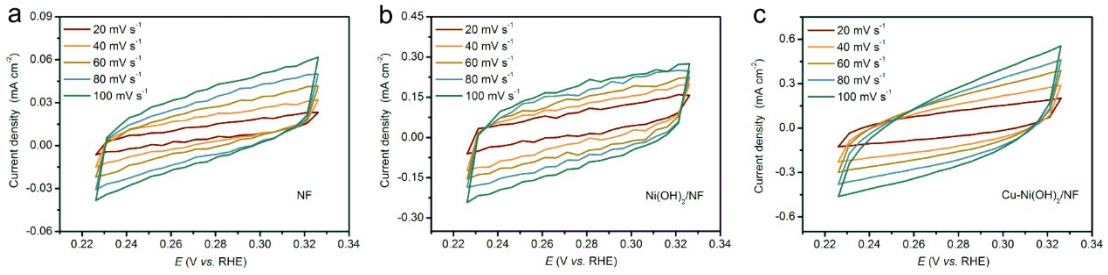

Fig. S4. (a-c) CV curves of NF, Ni(OH)$_2$/NF, and Cu-Ni(OH)$_2$/NF for ECSA and R_f evaluations.

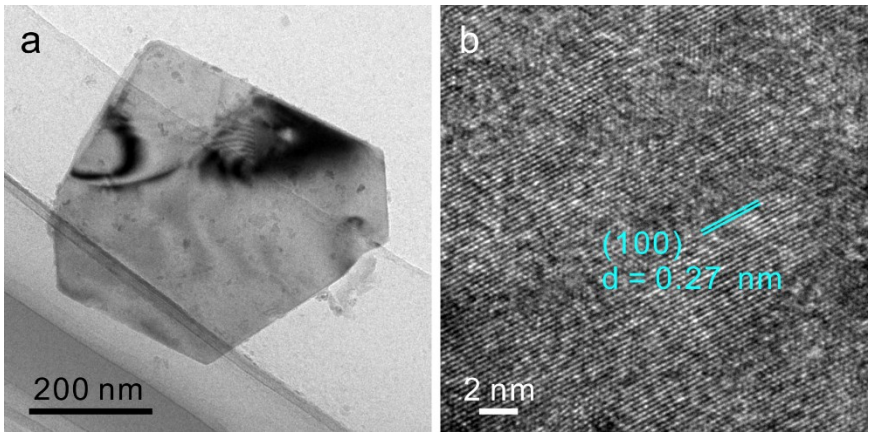

Fig. S5 The (a) TEM and (b) HRTEM images of Cu-Ni(OH)$_2$ after the stability test.

Table S3. Comparisons of HER activity of the Cu-$Ni(OH)_2$/NF with some representative HER electrocatalysts recently reported in alkaline media.

Catalyst	Overpotential for 10 mA cm^{-2} (mV)	Tafel slope ($mV\ dec^{-1}$)	Reference
Cu-$Ni(OH)_2$/NF	**53** **209 (η_{100})**	**51**	**This work**
NiFe LDH/NF	59	62	[5]
Ni-$Ni(OH)_2$/NF	72	43	[6]
$Ni(OH)_2$–Fe_2P/Ti mesh	76	105	[7]
CoMnS@NiO/CC	125	147	[8]
Fe-$Ni(OH)_2$/NF	138	63	[9]
Ni/NiO/NF	120	114	[10]
Ni_8P_3/NF	130	58	[11]
NiCo LDH/CC	367	40	[12]
NiCoS/Ti foil	88	118	[13]

Table S4. Corresponding results of ESCA and Roughness Factor.

Sample	ESCA (cm^2)	Roughness Factor
NF	1.0	6.5
$Ni(OH)_2$/NF	5.2	34.0
Cu-$Ni(OH)_2$/NF	8.4	54.3

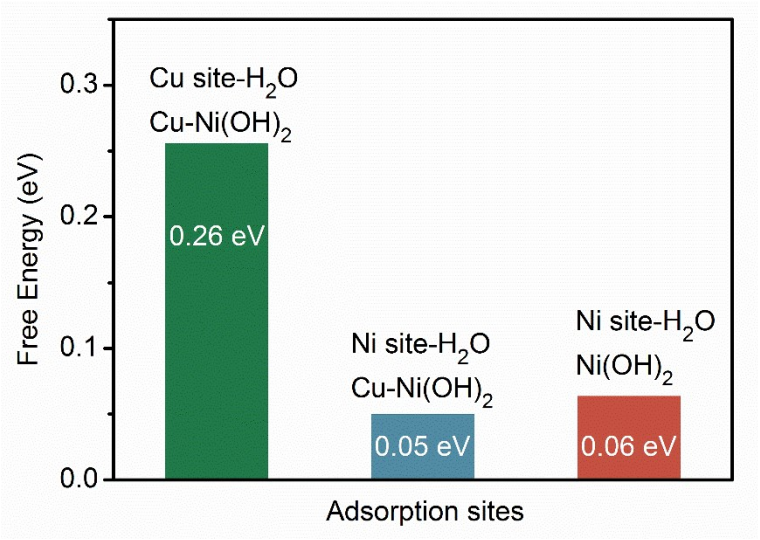

Fig. S6 Free energy of water molecule adsorption on different sites.

Table S5. The calculated free energies diagram.

Structure	ΔG (eV)
$Ni(OH)_2$-H_2O^*	0.06
$Ni(OH)_2$-Ts^*	2.73
$Ni(OH)_2$-H^*	0.49
Cu-$Ni(OH)_2$ (I)-H_2O^*	0.11
Cu-$Ni(OH)_2$ (I)-Ts^* (Ni-H)	2.33
Cu-$Ni(OH)_2$-H^* (Ni-H)	0.28
Cu-$Ni(OH)_2$ (II)-H_2O^*	0.05
Cu-$Ni(OH)_2$ (II)-Ts^* (Cu-H)	2.59
Cu-$Ni(OH)_2$-H^* (Cu-H)	1.57

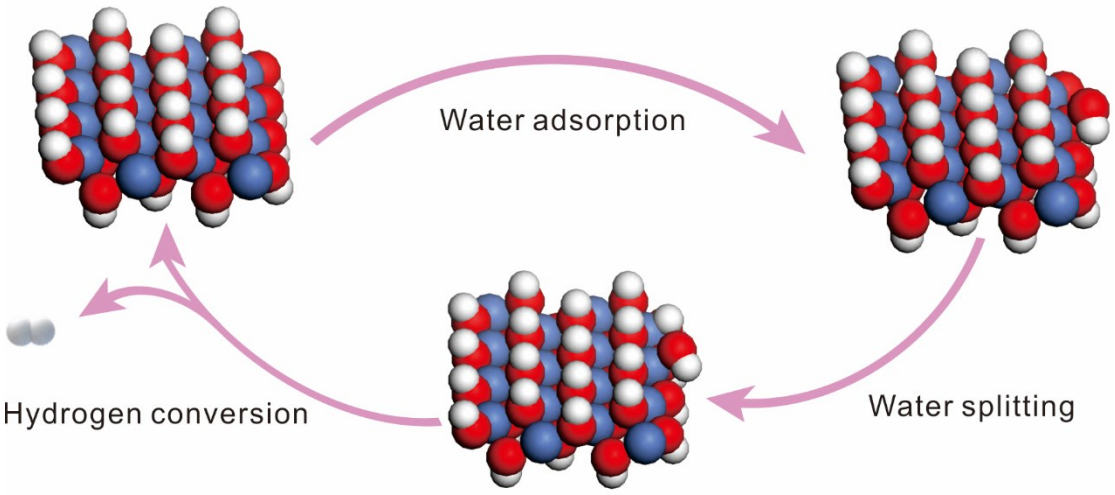

Fig. S7 The HER reaction pathway on $Ni(OH)_2$. Color scheme: white, H; red, O; blue, Ni.

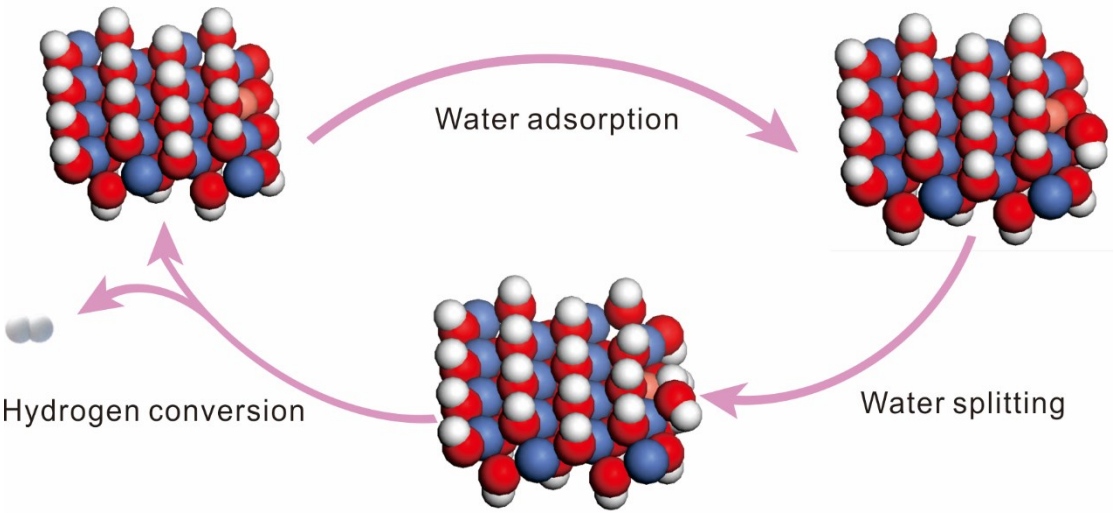

Fig. S8 The HER reaction pathway on Cu-Ni$(OH)_2$ (II). Color scheme: white, H; red, O; blue, Ni.

References:

1 Z. Jiang, X. Gu, L. Wang and L. Huang, *Chem. Phys. Lett.*, 2016, **659**, 230–233.

2 H. Xu, J. Wan, H. Zhang, L. Fang, L. Liu, Z. Huang, J. Li, X. Gu and Y. Wang, *Adv. Energy Mater.*, 2018, **8**, 1–7.

3 Z. Xing, L. Gan, J. Wang and X. Yang, *J. Mater. Chem. A*, 2017, **5**, 7744–7748.

4 M. J. Kolb, F. Calle-Vallejo, L. B. F. Juurlink and M. T. M. Koper, *J. Chem. Phys.*, 2014, **140**, 134708.

5 Z. Qiu, C.-W. Tai, G. A. Niklasson and T. Edvinsson, *Energy Environ. Sci.*, 2019, **12**, 572–581.

6 W. Zhong, W. Li, C. Yang, J. Wu, R. Zhao, M. Idrees, H. Xiang, Q. Zhang and X. Li, *J. Energy Chem.*, , DOI:10.1016/j.jechem.2021.02.013.

7 X. Zhang, S. Zhu, L. Xia, C. Si, F. Qu and F. Qu, *Chem. Commun.*, 2018, **54**, 1201–1204.

8 Q. Li, Z. Xing, D. Wang, X. Sun and X. Yang, *ACS Catal.*, 2016, **6**, 2797–2801.

9 J.-T. Ren, G.-G. Yuan, C.-C. Weng, L. Chen and Z.-Y. Yuan, *Nanoscale*, 2018, **10**, 10620–10628.

10 Y. Kuang, G. Feng, P. Li, Y. Bi, Y. Li and X. Sun, *Angew. Chemie Int. Ed.*, 2016, **55**, 693–697.

11 G.-F. Chen, T. Y. Ma, Z.-Q. Liu, N. Li, Y.-Z. Su, K. Davey and S.-Z. Qiao, *Adv. Funct. Mater.*, 2016, **26**, 3314–3323.

12 H. Liang, F. Meng, M. Cabán-Acevedo, L. Li, A. Forticaux, L. Xiu, Z. Wang and S. Jin, *Nano Lett.*, 2015, **15**, 1421–1427.

13 Z. Peng, D. Jia, A. M. Al-Enizi, A. A. Elzatahry and G. Zheng, *Adv. Energy Mater.*, 2015, **5**, 1402031.